論文 / 著書情報
Article / Book Information

Title	In-plane-dominated vibration characteristics of piezoelectric thick circular plates based on higher-order plate theories
Authors	Ming Ji, Yi-Chuang Wu, Chien-Ching Ma
Citation	Journal of Mechanics, Volume 38, , Page 410–432
Pub. date	2022, 11
DOI	https://doi.org/10.1093/jom/ufac034
Copyright	Information is in the article.

Journal of Mechanics, 2022, **38**, 410–432
https://doi.org/10.1093/jom/ufac034
Regular Article

In-plane-dominated vibration characteristics of piezoelectric thick circular plates based on higher-order plate theories

Ming Ji[1,2], Yi-Chuang Wu[3] and Chien-Ching Ma[1,*]

[1]Department of Mechanical Engineering, National Taiwan University, Taipei, Taiwan, Republic of China
[2]Institute of Innovative Research, Tokyo Institute of Technology, Midori-ku, Yokohama, Japan
[3]Advanced Institute of Manufacturing with High-tech Innovations & Department of Mechanical Engineering, National Chung Cheng University, Minhsiung, Chiayi, Republic of China

[*]Corresponding author: ccma@ntu.edu.tw

ABSTRACT

Numerous engineering applications exist for the piezoelectric effect, which results from the electromechanical coupling between electrical and mechanical fields. In-plane vibrations of piezoelectric plates' resonance frequencies and associated mode shapes have been thoroughly investigated. However, analytical solutions for in-plane-dominated vibrations of thick piezoelectric circular plates are limited. In this paper, higher-order plate theories for the in-plane-dominated vibration characteristics of piezoelectric circular thick plates under fully clamped and completely free boundary conditions are presented. The resonant frequencies and associated mode shapes were investigated based on two higher-order plate theories: second-order shear deformation plate theory and third-order shear deformation plate theory, as well as simplified third-order linear piezoelectric theory. Hamilton's principle was applied to derive equations of motion and boundary conditions. In the theoretical analysis, the resonant frequencies, associated mode shapes and distribution of electric displacements for various radius-to-thickness ratios were calculated. The numerical results obtained by the finite element method were compared with those obtained from theoretical analysis. Excellent agreement was found between the theoretical and numerical results for the thick piezoelectric circular plates.

KEYWORDS: piezoelectric thick circular plates, in-plane-dominated vibration, higher-order shear deformation plate theory, Hamilton's principle

1. INTRODUCTION

The piezoelectric effect has many engineering applications owing to the electromechanical coupling between the electrical and mechanical fields. Piezoelectric transducers, which are widely used in non-destructive testing, are primarily made of piezoelectric circular ceramics. High-frequency vibrations are the basis of nondestructive testing. Moreover, the resonant frequencies of in-plane-dominated vibrations are higher than those of out-of-plane-dominated vibrations. Thus, understanding the in-plane-dominated vibration characteristics of piezoelectric discs is crucial for designing transducers.

Based on Mindlin's [1] piezoelectric plate equations considering electric potential, rotatory inertia and shear deformations, Tiersten and Mindlin [2] derived more general equations for piezoelectric plates considering extensional modes. Holland [3] presented a theoretical study on the extensional modes of rectangular piezoelectric plates using variational techniques. Schmidt [4] investigated the extensional vibration of a circular piezoelectric plate covered by concentric circular electrodes both theoretically and experimentally. Schmidt [5] applied the finite element method (FEM) to the extensional vibrations of piezoelectric plates. Ikegami *et al.* [6] observed the fundamental thickness extensional mode of the $PbTiO_3$ piezoelectric ceramics. Ueha *et al.* [7] used an optical heterodyne technique to measure the velocity distributions along the radial direction of thick disks of $Pb\,(Zr\cdot Ti)O_3$. Locke *et al.* [8] used the FEM to calculate the natural vibrational modes of piezoelectric ceramic disks, including thickness extensional modes. Ohnishi *et al.* [9] presented a piezoelectric transformer operating in the second thickness extensional vibration mode for power supply. Guo *et al.* [10] predicted the vibration characteristics of piezoelectric discs with finite diameter-to-thickness ratios by using the FEM. The electrical impedance response and resonant frequencies were measured experimentally. Lee and Edwards [11] derived approximate second-order governing equations of extensional vibrations for piezoelectric plates, deduced from 3D equations of linear piezoelectricity. Huang *et al.* [12] presented approximate second-order equations for extensional, thickness-stretch, and symmetric thickness-shear vibrations of piezoelectric ceramic plates with electroded faces. Ma and Huang applied amplitude-fluctuation electronic speckle pattern interferometry (AF-ESPI) to measure the out-of-plane and in-plane modes of rectangular [13, 14] and circular [15] piezoceramic plates. Lin and Ma [16] designed partial electrodes to study the out-of-plane and in-plane motions of piezoceramic disks using three experimental methods: AF-ESPI, laser Doppler vibrometer-dynamic signal analyzer, and impedance analysis. Huang *et al.* [17] theoretically, numerically, and experimentally investigated the out-of-plane and in-plane vibration characteristics of the piezoelectric

Received: 13 September 2022; **Accepted:** 11 October 2022

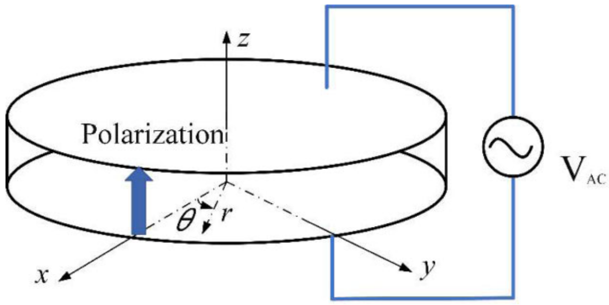

Figure 1 A geometric piezoelectric circular plate continuum.

disks. The thin plate theory was used in the theoretical analysis. Ma *et al.* [18] experimentally and numerically studied the in-plane vibration characteristics of piezoceramic and piezolaminated composite plates. Huang *et al.* [19] applied the Mindlin plate theory to study the transverse and planar vibrations of piezoceramic disks. Chillara *et al.* [20] studied the in-plane vibration characteristics of non-uniformly polarized rectangular piezoelectric wafers under the generalized plane stress assumption. Lin *et al.* [21] investigated both the steady-state and transient dynamic characteristics of polyvinylidene fluoride (PVDF) piezoelectric polymers. In steady-state vibration, the visible resonant mode fringe patterns are obtained using the amplitude-fluctuation electronic speckle pattern interferometry technique, and the point-wise displacement data are measured by laser Doppler vibrometer–dynamic signal analysis. The sensing ability of impact loading history was proved through the transient dynamic experiment by using two PVDFs on the cantilever beam. By employing piezoelectric theory with thermal effects and von Kármán nonlinear plate theory, the constitutive equations of the boron nitride nanotube (BNNT)-reinforced piezoelectric plate under complex load were studied by Yang *et al.* [22]. The numerical results show that decreasing voltage and temperature and increasing volume ratio can delay the chaotic or multiple periodic motions of BNNT-reinforced piezoelectric plates, thus improving the dynamic stability of the structure. Thick piezoelectric plates can be any shape and used as a piezoelectric actuator, piezoelectric sensor, or piezoelectric transducer. These thick piezoelectric plates are commonly used for high-power applications and generation, or ultrasonic sensory applications. High-power ultrasonic scalers/cleaners are the most widely used application for thick piezoelectric plates. The thicker the plate, the more power it will generate as a cleaner.

Although the resonant frequencies and associated mode shapes of the in-plane vibration of piezoelectric plates have been extensively investigated, analytical solutions for in-plane-dominated vibrations of thick piezoelectric circular plates, especially with completely free boundary conditions, are limited. In this paper, two higher-order plate theories, second-order shear deformation plate theory (SSDT) and third-order shear deformation plate theory (TSDT), and simplified third-order linear piezoelectric theory are presented to study the in-plane dominated vibrations of thick piezoelectric circular plates under fully clamped and completely free boundary conditions. Hamilton's principle was applied to derive equations of motion and boundary conditions. In the theoretical analysis, the resonant frequencies and associated mode shapes for various radius-to-thickness ratios were calculated. The numerical results obtained by the FEM were compared with those obtained from theoretical analysis.

2. SECOND-ORDER SHEAR DEFORMATION PLATE MODEL

Fig. 1 depicts a circular piezoelectric plate with radius R and thickness $H = 2h$ specified in a cylindrical coordinate system (r, θ, z). According to the linear piezoelectric hypothesis

$$\begin{cases} \sigma_{ij} = C^E_{ijkl}\varepsilon_{kl} - e_{kij}E_k \\ D_i = e_{ikl}\varepsilon_{kl} + \varepsilon^S_{ij}E_j \end{cases}, \tag{1}$$

where σ_{ij} and ε_{kl} are the stress and strain, respectively, and E_j and D_i are the electric field and displacement, respectively. The coefficients of C^E_{ijkl}, e_{ikl}, and ε^S_{ij} are the elastic stiffness, piezoelectric coefficient, and dielectric coefficient, respectively. The piezoelectric material is a crystal symmetry class C_{6mm}. The constitutive equations in matrix notation can be rewritten as:

$$\begin{bmatrix} \sigma_{rr} \\ \sigma_{\theta\theta} \\ \sigma_{zz} \\ \sigma_{\theta z} \\ \sigma_{zr} \\ \sigma_{r\theta} \\ D_r \\ D_\theta \\ D_z \end{bmatrix} = \begin{bmatrix} C^E_{11} & C^E_{12} & C^E_{13} & 0 & 0 & 0 & 0 & 0 & -e_{31} \\ C^E_{12} & C^E_{11} & C^E_{13} & 0 & 0 & 0 & 0 & 0 & -e_{31} \\ C^E_{13} & C^E_{13} & C^E_{33} & 0 & 0 & 0 & 0 & 0 & -e_{33} \\ 0 & 0 & 0 & C^E_{55} & 0 & 0 & 0 & -e_{15} & 0 \\ 0 & 0 & 0 & 0 & C^E_{55} & 0 & -e_{15} & 0 & 0 \\ 0 & 0 & 0 & 0 & 0 & \frac{1}{2}\left(C^E_{11} - C^E_{12}\right) & 0 & 0 & 0 \\ 0 & 0 & 0 & 0 & e_{15} & 0 & \varepsilon^S_{11} & 0 & 0 \\ 0 & 0 & 0 & e_{15} & 0 & 0 & 0 & \varepsilon^S_{11} & 0 \\ e_{31} & e_{31} & e_{33} & 0 & 0 & 0 & 0 & 0 & \varepsilon^S_{33} \end{bmatrix} \begin{bmatrix} \varepsilon_{rr} \\ \varepsilon_{\theta\theta} \\ \varepsilon_{zz} \\ \gamma_{\theta z} \\ \gamma_{zr} \\ \gamma_{r\theta} \\ E_r \\ E_\theta \\ E_z \end{bmatrix}. \tag{2}$$

The elastic stiffness and piezoelectric coefficients can be shortened using Voigt notation, and the elastic and piezoelectric constants can be rewritten as C_{pq}^{E} and e_{iq}, respectively. The subscripts range of p and q are from 1 to 6.

The SSDT was used to study the in-plane-dominated vibration of a piezoelectric circular plate. The form of displacement assumption can be given as following:

$$u_r(r,\theta,z,t) = u_0(r,\theta,t) - \frac{z^2}{2}\frac{\partial w(r,\theta,t)}{\partial r}, \tag{3}$$

$$u_\theta(r,\theta,z,t) = v_0(r,\theta,t) - \frac{z^2}{2}\frac{1}{r}\frac{\partial w(r,\theta,t)}{\partial \theta}, \tag{4}$$

$$u_z(r,\theta,z,t) = zw(r,\theta,t), \tag{5}$$

where u_0 and v_0 are the in-plane displacements of the mid-plane, and w is the normal strain along the thickness direction. The strain–displacement relations are

$$\begin{aligned} &\varepsilon_{rr} = \frac{\partial u_r}{\partial r}, \quad \varepsilon_{\theta\theta} = \frac{u_r}{r} + \frac{1}{r}\frac{\partial u_\theta}{\partial \theta}, \quad \varepsilon_{zz} = \frac{\partial u_z}{\partial z} \\ &\gamma_{r\theta} = \frac{1}{r}\frac{\partial u_r}{\partial \theta} + \frac{\partial u_\theta}{\partial r} - \frac{u_\theta}{r}, \quad \gamma_{rz} = \frac{\partial u_r}{\partial z} + \frac{\partial u_z}{\partial r}, \quad \gamma_{\theta z} = \frac{\partial u_\theta}{\partial z} + \frac{1}{r}\frac{\partial u_z}{\partial \theta}. \end{aligned} \tag{6}$$

The electrostatic equation can also be given by

$$\frac{\partial D_r}{\partial r} + \frac{D_r}{r} + \frac{1}{r}\frac{\partial D_\theta}{\partial \theta} + \frac{\partial D_z}{\partial z} = 0. \tag{7}$$

The electric field–electric potential relations are

$$E_r = -\frac{\partial \phi}{\partial r}, \quad E_\theta = -\frac{1}{r}\frac{\partial \phi}{\partial \theta}, \quad E_z = -\frac{\partial \phi}{\partial z}, \tag{8}$$

where ϕ is the electric potential.

The electric potential is assumed to be a cubic equation of z.

$$\phi\,(r,\theta,z,t) = \phi^{(0)}\,(r,\theta,t) + z\phi^{(1)}\,(r,\theta,t) + z^2\phi^{(2)}\,(r,\theta,t) + z^3\phi^{(3)}\,(r,\theta,t)\,, \tag{9}$$

where $\phi^{(i)}$ is the i-th order electric potential.

Considering the electrical potential boundary on two electrode surfaces, it can be represented as

$$\phi|_{z=\pm h} = \pm V e^{i\omega t}. \tag{10}$$

Electrodes for the piezoelectric plate were laid on the top and bottom surfaces, and the lateral surfaces were all free of electrodes. Thus, the in-plane electric displacements D_r and D_θ are negligible compared with the out-of-plane electric displacement D_z. Using the above assumption, the electric potential can be written as the following equation from Eqs. (8) to (12).

$$\phi = \frac{zV}{h}e^{i\omega t} + \frac{e_{31}h^2}{6\varepsilon_{33}^{S}}\left(z - \frac{z^3}{h^2}\right)\Delta w, \tag{11}$$

where $\Delta = \frac{\partial^2}{\partial r^2} + \frac{1}{r}\frac{\partial}{\partial r} + \frac{1}{r^2}\frac{\partial^2}{\partial \theta^2}$. The electric fields can be expressed as

$$E_r = -\frac{e_{15}}{\varepsilon_{11}^{S}}\gamma_{rz}, \tag{12}$$

$$E_\theta = -\frac{e_{15}}{\varepsilon_{11}^{S}}\gamma_{\theta z}, \tag{13}$$

and

$$E_z = -\frac{V}{h}e^{i\omega t} - \frac{e_{31}h^2}{6\varepsilon_{33}^{S}}\left(1 - \frac{3z^2}{h^2}\right)\Delta w. \tag{14}$$

Hamilton's principle in control volume V and control surface S can be expressed as

$$\delta\tilde{K} + \delta\tilde{U} + \delta\tilde{W} + \delta\tilde{E} = 0, \tag{15}$$

where $\tilde{K}$ is the kinetic energy, $\tilde{U}$ is the work done by internal forces, $\tilde{W}$ is the work done by external forces, and $\tilde{E}$ is the work done by electric fields. From time $t = t_1$ to t_2, virtual variables can be expressed as

$$\delta\tilde{K} = \int_{t_1}^{t_2}\int_V \dot{u}_j\delta\dot{u}_j dVdt, \tag{16}$$

$$\delta\tilde{U} = -\int_{t_1}^{t_2}\int_V \sigma_{ij}\delta\varepsilon_{ij}dVdt, \tag{17}$$

$$\delta\tilde{W} = \int_{t_1}^{t_2}\int_s \tilde{t}_i\delta u_i + q\delta\phi dSdt, \tag{18}$$

and

$$\delta\tilde{E} = -\int_{t_1}^{t_2}\int_s D_i\delta E_i dVdt, \tag{19}$$

where $\tilde{t}_i$ is the traction on the control surface and q is the electric charge on the control surface. The equations of motion can be derived from Hamilton's principle.

$$\frac{Q_1 - Q_2}{r} + \frac{\partial Q_1}{\partial r} - \frac{1}{r}\frac{\partial Q_6}{\partial \theta} = I_1\ddot{u}_0 - \frac{I_3}{2}\frac{\partial \ddot{w}}{\partial r}, \tag{20}$$

$$\frac{1}{r}\frac{\partial Q_2}{\partial \theta} + \frac{\partial Q_6}{\partial r} + \frac{2Q_6}{r} = I_1\ddot{v}_0 - \frac{I_3}{2}\frac{1}{r}\frac{\partial \ddot{w}}{\partial \theta}, \tag{21}$$

$$\frac{2}{r}\frac{\partial R_1}{\partial r} + \frac{\partial^2 R_1}{\partial r^2} - \frac{1}{r}\frac{\partial R_2}{\partial r} + \frac{1}{r^2}\frac{\partial^2 R_2}{\partial \theta^2} + \frac{2}{r}\frac{\partial^2 R_6}{\partial r\partial \theta} + \frac{2}{r^2}\frac{\partial R_6}{\partial \theta} - 2Q_3 = I_3\ddot{\Psi} - \frac{I_5}{2}\Delta\ddot{w} + 2I_3\ddot{w}, \tag{22}$$

where $(I_1, I_3, I_5) = \int_{-h}^{h}\rho(1, z^2, z^4)dz$; $Q_i = \int_{-h}^{h}\sigma_i dz$; $R_i = \int_{-h}^{h}\sigma_i z^2 dz$, for i = 1,2,3,6; $(\sigma_1,\sigma_2,\sigma_3,\sigma_6)$ represent $(\sigma_{rr},\sigma_{\theta\theta},\sigma_{zz},\sigma_{r\theta})$, respectively. The clamped boundary conditions can be expressed as

$$w\,|_{r=R} = \frac{\partial w}{\partial r}\,|_{r=R} = u_0\,|_{r=R} = v_0\,|_{r=R} = 0. \tag{23}$$

The free boundary conditions can be expressed as

$$\left.\frac{R_1 - R_2}{r} + \frac{\partial R_1}{\partial r} + \frac{2}{r}\frac{\partial R_6}{\partial \theta} - \left(I_3\ddot{u}_0 - \frac{I_5}{2}\frac{\partial \ddot{w}}{\partial r}\right)\right|_{r=R} = R_1|_{r=R} = Q_1|_{r=R} = Q_6|_{r=R} = 0. \tag{24}$$

The non-dimensional terms introduced are $\xi = r/R$, $\eta = h/R$, $\overline{w} = w$, $\bar{u}_0 = u_0/R$, $\bar{v}_0 = v_0/R$, $\lambda^4 = (\omega^2R^2\rho)/C_{11}^E$, and ω represents the angular frequency. The procedure for solving the equations of motion was the same as in [23]. The solutions can be expressed as

$$\bar{w} = \left(\sum_{i=1}^{3} C_i\hat{w}_{in}(\alpha_i\xi)\right)\cos(n\theta)e^{i\omega t}, \tag{25}$$

$$\hat{u}_0 = \left(\sum_{i=1}^{3} C_i\chi_i\frac{\partial \hat{w}_{in}}{\partial \xi} + C_4\frac{n}{\xi}\hat{w}_{4n}\right)\cos(n\theta)e^{i\omega t}, \tag{26}$$

$$\hat{v}_0 = \left(-\sum_{i=1}^{3} C_i\chi_i\frac{n}{\xi}\hat{w}_{in} - C_4\frac{\partial \hat{w}_{4n}}{\partial \xi}\right)\sin(n\theta)e^{i\omega t}, \tag{27}$$

where

$$\hat{w}_{in}(\alpha_i\xi) = \begin{cases} J_n(\alpha_i\xi), & x_i < 0 \\ I_n(\alpha_i\xi), & x_i > 0 \end{cases} \quad i = 1-3, \tag{28}$$

$$\alpha_i = \sqrt{|x_i|}, \tag{29}$$

and

$$\chi_i = \frac{\eta^2}{6} - \frac{\gamma_{13}}{x_i + \lambda^4}. \tag{30}$$

The coefficients x_1 to x_3 are the solutions of the cubic equation

$$\tilde{P}_1x^3 + \tilde{P}_2x^2 + \tilde{P}_3x + \tilde{P}_4 = 0 \tag{31}$$

The parameters in Eq. (33) are defined as

$$\tilde{P}_1 = W_{11}Z_{21} - W_{21}Z_{11},\quad \tilde{P}_2 = W_{11}Z_{22} + W_{12}Z_{21} - W_{21}Z_{12} - W_{22}Z_{11},$$
$$\tilde{P}_3 = W_{11}Z_{23} + W_{12}Z_{22} - W_{22}Z_{12},\quad \tilde{P}_4 = W_{12}Z_{23},\quad W_{11} = 1,\quad W_{12} = \lambda^4,\quad W_{21} = 1,$$
$$W_{22} = \lambda^4 - \frac{6\gamma_{13}}{\eta^2},\quad Z_{11} = -\frac{\eta^2}{6},\quad Z_{12} = \gamma_{13} - \frac{\eta^2}{6}\lambda^4,\quad Z_{21} = -\left(\frac{3}{10} + \frac{4}{5}n_{31}\right)\eta^2,$$
$$Z_{22} = 2\gamma_{13} - \frac{3}{10}\eta^2\lambda^4,\quad Z_{23} = 2\lambda^4 - \frac{6\gamma_{33}}{\eta^2},\quad \gamma_{12} = \frac{C_{12}^E}{C_{11}^E},\quad \gamma_{13} = \frac{C_{13}^E}{C_{11}^E},$$
$$\gamma_{55} = \frac{C_{55}^E}{C_{11}^E},\quad \text{and}\quad n_{31} = \frac{e_{31}^2}{6C_{11}^E\varepsilon_{33}^S}.$$

The coefficient x_4 is expressed as

$$x_4 = -\frac{2\lambda^4}{1-\gamma_{12}} \tag{32}$$

By substituting the solutions into the boundary conditions, the algebraic equations can be written in a matrix form as

$$\begin{bmatrix} S_{11}^S & S_{12}^S & S_{13}^S & S_{14}^S \\ S_{21}^S & S_{22}^S & S_{23}^S & S_{24}^S \\ S_{31}^S & S_{32}^S & S_{33}^S & S_{34}^S \\ S_{41}^S & S_{42}^S & S_{43}^S & S_{44}^S \end{bmatrix} \begin{bmatrix} C_1 \\ C_2 \\ C_3 \\ C_4 \end{bmatrix} = \begin{bmatrix} 0 \\ 0 \\ 0 \\ 0 \end{bmatrix} \tag{33}$$

The matrix elements S_{ij}^S under clamped boundary conditions and free boundary conditions are provided in Appendix A. The resonant frequencies determine the determinant of the matrix in Eq. (35) to be zero.

3. THIRD-ORDER SHEAR DEFORMATION PLATE MODEL

The displacement fields of third-order shear deformation plate model can be expressed as

$$u_r(r,\theta,z,t) = u_0(r,\theta,t) - \frac{z^2}{2}\frac{\partial w(r,\theta,t)}{\partial r} - \frac{z^2h^2}{2}\frac{\partial \psi_z(r,\theta,t)}{\partial r} \tag{34}$$

$$u_\theta(r,\theta,z,t) = v_0(r,\theta,t) - \frac{z^2}{2}\frac{1}{r}\frac{\partial w(r,\theta,t)}{\partial \theta} - \frac{z^2h^2}{2}\frac{1}{r}\frac{\partial \psi_z(r,\theta,t)}{\partial \theta} \tag{35}$$

and

$$u_z(r,\theta,z,t) = zw(r,\theta,t) + z^3\psi_z(r,\theta,t) \tag{36}$$

where w is the first-order transverse displacement, ψ_z is the third-order transverse displacement and u_0 and v_0 are the in-plane displacements of the midplane. The electric potential can be expressed by

$$\phi = \frac{zV}{h}e^{i\omega t} - h^2\left(z - \frac{z^3}{h^2}\right)\left[\frac{e_{33}}{\varepsilon_{33}^S}\psi_z - \frac{e_{31}}{6\varepsilon_{33}^S}(\Delta w + h^2\Delta\psi_z)\right] \tag{37}$$

The electric fields can be expressed as

$$E_r = -\frac{e_{15}}{\varepsilon_{11}^S}\gamma_{rz} \tag{38}$$

$$E_\theta = -\frac{e_{15}}{\varepsilon_{11}^S}\gamma_{\theta z} \tag{39}$$

and

$$E_z = -\frac{V}{h}e^{i\omega t} + h^2\left(1 - \frac{3z^2}{h^2}\right)\left[\frac{e_{33}}{\varepsilon_{33}^S}\psi_z - \frac{e_{31}}{6\varepsilon_{33}^S}(\Delta w + h^2\Delta\psi_z)\right] \tag{40}$$

Using Hamilton's principles, the equations of motion can be obtained.

$$\frac{Q_1 - Q_2}{r} + \frac{\partial Q_1}{\partial r} - \frac{1}{r}\frac{\partial Q_6}{\partial \theta} = I_1\ddot{u}_0 - \frac{I_3}{2}\frac{\partial \ddot{w}}{\partial r} - \frac{I_3h^2}{2}\frac{\partial \ddot{\psi}_z}{\partial r} \tag{41}$$

$$\frac{1}{r}\frac{\partial Q_2}{\partial \theta}+\frac{\partial Q_6}{\partial r}+\frac{2Q_6}{r}=I_1\ddot{v}_0-\frac{I_3}{2}\frac{1}{r}\frac{\partial \ddot{w}}{\partial \theta}-\frac{I_3h^2}{2}\frac{1}{r}\frac{\partial \ddot{\psi}_z}{\partial \theta} \tag{42}$$

$$\begin{aligned}&\frac{2}{r}\frac{\partial R_1}{\partial r}+\frac{\partial^2 R_1}{\partial r^2}-\frac{1}{r}\frac{\partial R_2}{\partial r}+\frac{1}{r^2}\frac{\partial^2 R_2}{\partial \theta^2}+\frac{2}{r}\frac{\partial^2 R_6}{\partial r\partial \theta}+\frac{2}{r^2}\frac{\partial R_6}{\partial \theta}-2Q_3\\ &=I_3\ddot{\Psi}-\frac{I_5}{2}\Delta\ddot{w}-\frac{I_5h^2}{2}\Delta\ddot{\psi}_z+2I_3\ddot{w}+2I_5\ddot{\psi}_z\end{aligned} \tag{43}$$

$$\begin{aligned}&\frac{1}{r}\frac{\partial M_4}{\partial \theta}-\frac{1}{h^2}\frac{1}{r}\frac{\partial P_4}{\partial \theta}+\frac{\partial M_5}{\partial r}-\frac{1}{h^2}\frac{\partial P_5}{\partial r}+\frac{M_5}{r}-\frac{1}{h^2}\frac{P_5}{r}-Q_3+\frac{3R_3}{h^2}\\ &=\left(I_3-\frac{I_5}{h^2}\right)\ddot{w}+\left(I_5-\tfrac{I_7}{h^2}\right)\ddot{\psi}_z\end{aligned} \tag{44}$$

where $(I_1, I_3, I_5, I_7)=\int_{-h}^{h}\rho(1, z^2, z^4, z^6)dz$; $Q_i=\int_{-h}^{h}\sigma_i dz$; $R_i=\int_{-h}^{h}\sigma_i z^2 dz$ for $i=1, 2, 3, 6$; $M_i=\int_{-h}^{h}\sigma_i z dz$; $P_i=\int_{-h}^{h}\sigma_i z^3 dz$ for $i=4, 5$; $(\sigma_1,\sigma_2,\sigma_3,\sigma_4,\sigma_5,\sigma_6)$ represent $(\sigma_{rr},\sigma_{\theta\theta},\sigma_{zz},\sigma_{\theta z},\sigma_{rz},\sigma_{r\theta})$, respectively. The clamped boundary conditions can be expressed as

$$w\,|_{r=R}=\psi_z\,|_{r=R}=\frac{\partial w}{\partial r}+h^2\frac{\partial \psi_z}{\partial r}\,|_{r=R}=u_0\,|_{r=R}=v_0\,|_{r=R}=0. \tag{45}$$

The free boundary conditions can be expressed as

$$\begin{aligned}&\frac{\partial R_1}{\partial r}+\frac{R_1-R_2}{r}+\frac{2}{r}\frac{\partial R_6}{\partial \theta}-\left(I_3\ddot{u}_0-\frac{I_5}{2}\frac{\partial \ddot{w}}{\partial r}-\frac{I_5h^2}{2}\frac{\partial \ddot{\psi}_z}{\partial r}\right)\Bigg|_{r=R}\\ &=M_5-\frac{P_5}{h^2}\Bigg|_{r=R}=R_1|_{r=R}=Q_1|_{r=R}=Q_6|_{r=R}=0\end{aligned} \tag{46}$$

The non-dimensional variables introduced are $\xi=r/R$, $\eta=h/R$, $\overline{w}=w$, $\bar{\psi}_z=R^2\psi_z$, $\bar{u}_0=u_0/R$, $\bar{v}_0=v_0/R$, and $\lambda^4=(\omega^2R^2\rho)/C_{11}^E$. The solutions can be expressed as

$$\bar{w}=\left(\sum_{i=1}^{4}C_i\hat{w}_{in}(\alpha_i\xi)\right)\cos(n\theta)e^{i\omega t} \tag{47}$$

$$\bar{\psi}_z=\left(\sum_{i=1}^{4}C_i\lambda_i\hat{w}_{in}(\alpha_i\xi)\right)\cos(n\theta)e^{i\omega t} \tag{48}$$

$$\bar{u}_0=\left(\sum_{i=1}^{4}C_i\chi_i\frac{\partial \hat{w}_{in}}{\partial \xi}+C_5\frac{n}{\xi}\hat{w}_{5n}\right)\cos(n\theta)e^{i\omega t} \tag{49}$$

and

$$\bar{v}_0=\left(-\sum_{i=1}^{4}C_i\chi_i\frac{n}{\xi}\hat{w}_{in}-C_5\frac{\partial \hat{w}_{5n}}{\partial \xi}\right)\sin(n\theta)e^{i\omega t} \tag{50}$$

where

$$\hat{w}_{in}(\alpha_i\xi)=\begin{cases}J_n(\alpha_i\xi), & x_i<0\\ I_n(\alpha_i\xi), & x_i>0\end{cases}\quad i=1-5 \tag{51}$$

$$\alpha_i=\sqrt{|x_i|} \tag{52}$$

$$\lambda_i=-\frac{W_{31}x_i+W_{32}}{Z_{31}x_i+Z_{32}} \tag{53}$$

and

$$\chi_i=\frac{\eta^2}{6}+\frac{\eta^4\lambda_i}{6}-\frac{\gamma_{13}(1+\eta^2\lambda_i)}{x_i+\lambda^4} \tag{54}$$

The coefficients x_1 to x_4 are the solutions of the biquadratic equation.

$$\tilde{P}_1x^4+\tilde{P}_2x^3+\tilde{P}_3x^2+\tilde{P}_4x+\tilde{P}_5=0 \tag{55}$$

Table 1 Material Constants of Piezoceramics PSI-5A4E (Piezo System Incorporation).

Material properties		**Values**
Density $(\mathrm{kg/m^3})$	ρ	7800
Elastic constants (GPa)	C_{11}^E	80.4
	C_{12}^E	30.0
	C_{13}^E	21.1
	C_{33}^E	60.0
	C_{55}^E	15.9
Piezoelectric stress constants (C/m^2)	e_{15}	8.77
	e_{31}	−12.77
	e_{33}	15.41
Dielectric constants $(10^{-9}F/m)$	ε_{11}^S	11.12
	ε_{33}^S	5.08

The parameters in Eq. (57) are defined as

$$\tilde{P}_1 = W_{31}\left(Z_{11} - Z_{21}\right) - Z_{31}\left(W_{11} - W_{21}\right),$$
$$\tilde{P}_2 = W_{31}\left(Z_{12} + Y_{22}Z_{11} - Z_{22} - Y_{12}Z_{21}\right) + W_{32}\left(Z_{11} - Z_{21}\right)$$
$$-Z_{31}\left(W_{12} + Y_{22}W_{11} - W_{22} - Y_{12}W_{21}\right) - Z_{32}\left(W_{11} - W_{21}\right),$$
$$\tilde{P}_3 = W_{31}\left(Y_{22}Z_{12} - Z_{23} - Y_{12}Z_{22}\right) + W_{32}\left(Z_{12} + Y_{22}Z_{11} - Z_{22} - Y_{12}Z_{21}\right)$$
$$-Z_{31}\left(Y_{22}W_{12} - W_{23} - Y_{12}W_{22}\right) - Z_{32}\left(W_{12} + Y_{22}W_{11} - W_{22} - Y_{12}W_{21}\right),$$
$$\tilde{P}_4 = -W_{31}Y_{12}Z_{23} + W_{32}\left(Y_{22}Z_{12} - Z_{23} - Y_{12}Z_{22}\right) + Z_{31}Y_{12}W_{23} - Z_{32}\left(Y_{22}W_{12} - W_{23} - Y_{12}W_{22}\right),$$
$$\tilde{P}_5 = -W_{32}Y_{12}Z_{23} + Z_{32}Y_{12}W_{23}, \quad Y_{11} = 1, \quad Y_{12} = \lambda^4, \quad Y_{21} = 1, \quad Y_{22} = \lambda^4 - \frac{6\gamma_{13}}{\eta^2} \quad W_{11} = -\frac{\eta^2}{6}, \quad W_{12} = \gamma_{13} - \frac{\eta^2}{6}\lambda^4,$$
$$W_{21} = -\left(\frac{3}{10} + \frac{2}{15}m_2\right)\eta^2, \quad W_{22} = 2\gamma_{13} - \frac{3}{10}\eta^2\lambda^4, \quad W_{23} = 2\lambda^4 - \frac{6\gamma_{33}}{\eta^2}, \quad Z_{11} = -\frac{\eta^4}{6}, \quad Z_{12} = \left(\gamma_{13} - \frac{\eta^2}{6}\lambda^4\right)\eta^2,$$
$$Z_{21} = -\left(\frac{3}{10} + \frac{2}{15}m_2\right)\eta^4, \quad Z_{22} = \left(\frac{14}{5}\gamma_{13} + \frac{4}{5}m_1 - \frac{3}{10}\eta^2\lambda^4\right)\eta^2, \quad Z_{23} = \frac{6}{5}\eta^2\lambda^4 - 6\gamma_{33}, \quad \gamma_{12} = \frac{C_{12}^E}{C_{11}^E}, \quad \gamma_{13} = \frac{C_{13}^E}{C_{11}^E},$$
$$\gamma_{55} = \frac{C_{55}^E}{C_{11}^E}, \quad m_1 = \frac{e_{31}e_{33}}{C_{11}^E\varepsilon_{33}^S}, \quad m_2 = \frac{e_{31}^2}{C_{11}^E\varepsilon_{33}^S}, \quad m_3 = \frac{e_{15}^2}{C_{11}^E\varepsilon_{11}^S}, \quad \text{and} \quad m_4 = \frac{e_{33}^2}{C_{11}^E\varepsilon_{33}^S}.$$

The coefficient x_5 is expressed as

$$x_5 = -\frac{2\lambda^4}{1 - \gamma_{12}}. \tag{56}$$

By substituting the solutions into the boundary conditions, the algebraic equations can be written in a matrix form as

$$\begin{bmatrix} S_{11}^T & S_{12}^T & S_{13}^T & S_{14}^T & S_{15}^T \\ S_{21}^T & S_{22}^T & S_{23}^T & S_{24}^T & S_{25}^T \\ S_{31}^T & S_{32}^T & S_{33}^T & S_{34}^T & S_{35}^T \\ S_{41}^T & S_{42}^T & S_{43}^T & S_{44}^T & S_{45}^T \\ S_{51}^T & S_{52}^T & S_{53}^T & S_{54}^T & S_{55}^T \end{bmatrix} \begin{bmatrix} C_1 \\ C_2 \\ C_3 \\ C_4 \\ C_5 \end{bmatrix} = \begin{bmatrix} 0 \\ 0 \\ 0 \\ 0 \\ 0 \end{bmatrix}. \tag{57}$$

The matrix elements S_{ij}^T under clamped and free boundary conditions are provided in Appendix B.

4. NUMERICAL RESULTS AND DISCUSSION

Theoretical and numerical calculations were carried out on a thick piezoceramic disk with a radius of 29 mm under fully clamped and completely free boundary conditions. The numerical findings were obtained using the commercial finite element program COMSOL Multiphysics and used to validate the theoretical results. The 3D element with finer mesh was used to guarantee precision and convergence of the numerical model. Two comparatively thick thicknesses, 2.9 and 5.8 mm, were used for the study. Table 1 contains a list of the piezoceramic PSI-5A4E (Piezo System Incorporation) material characteristics.

Table 2 The first ten natural frequencies (Hz) obtained from COMSOL and plate theories for a plate with clamped boundary conditions ($R/H = 10$).

Mode	(n, c)	COMSOL	SSDT	Error (%)	TSDT	Error (%)
1	(1,0)	32 826	32 878	0.1584	32 878	0.1584
2	(0,0)	37 791	37 791	0.0000	37 791	0.0000
3	(2,0)	51 063	51 150	0.1704	51 149	0.1684
4	(1,1)	53 007	53 009	0.0038	53 009	0.0038
5	(0,0)	64 375	64 485	0.1709	64 484	0.1693
6	(3,0)	66 322	66 425	0.1553	66 425	0.1553
7	(2,1)	68 202	68 219	0.0249	68 219	0.0249
8	(0,1)	69 193	69 193	0.0000	69 193	0.0000
9	(4,0)	79 857	79 964	0.1340	79 963	0.1327
10	(1,1)	83 552	83 564	0.0144	83 564	0.0144
11	(3,1)	83 946	84 003	0.0679	84 003	0.0679
12	(1,1)	90 065	90 210	0.1610	90 209	0.1599
13	(5,0)	92 433	92 541	0.1168	92 540	0.1158
14	(2,1)	97 711	97 714	0.0031	97 714	0.0031

Table 3 The first ten natural frequencies (Hz) obtained from COMSOL and plate theories for a plate with clamped boundary conditions ($R/H = 5$).

Mode	(n, c)	COMSOL	SSDT	Error (%)	TSDT	Error (%)
1	(1,0)	32 850	32 958	0.3288	32 957	0.3257
2	(0,0)	37 791	37 791	0.0000	37 791	0.0000
3	(2,0)	51 087	51 267	0.3523	51 266	0.3504
4	(1,1)	53 004	53 009	0.0094	53 009	0.0094
5	(0,0)	64 309	64 540	0.3592	64 538	0.3561
6	(3,0)	66 338	66 552	0.3226	66 551	0.3211
7	(2,1)	68 185	68 226	0.0601	68 226	0.0601
8	(0,1)	69 193	69 193	0.0000	69 193	0.0000
9	(4,0)	79 864	80 087	0.2792	80 086	0.2780
10	(1,1)	83 526	83 552	0.0311	83 551	0.0299
11	(3,1)	83 886	84 025	0.1657	84 024	0.1645
12	(1,1)	89 793	90 114	0.3575	90 110	0.3530
13	(5,0)	92 434	92 658	0.2423	92 657	0.2413
14	(2,1)	97 674	97 681	0.0072	97 681	0.0072

Tables 2 and 3 show the resonant frequencies of the in-plane dominated modes under 100 000 Hz obtained from COMSOL, SSDT and TSDT of a piezoceramic plate with fully clamped boundary conditions and different radius-to-thickness ratios ($R/H = 10$ and 5). Here, the error $= |f_{Theory} - f_{COMSOL}|/f_{COMSOL} \times 100\%$; mode indices n and c represent the number of nodal lines and nodal circles, respectively. Tables 4 and 5 show the resonant frequencies of the in-plane dominated modes under 100 000 Hz obtained from COMSOL, SSDT and TSDT of a piezoceramic plate with completely free boundary conditions and different radius-to-thickness ratios ($R/H = 10$ and 5). The two high-order shear-deformation plate theories can accurately predict the resonant frequencies of thick piezoelectric plates. Thickness has a significant effect on the error between the theoretical and numerical results. The error between the theoretical and numerical results increases with increasing thickness. In Table 2, the absolute errors for the SSDT and TSDT are < 0.1709% and 0.1693%, respectively. In Table 3, the absolute errors for the SSDT and TSDT are < 0.3592% and 0.3561%, respectively. In Table 4, the absolute errors for the SSDT and TSDT are < 0.6190% and 0.0010%, respectively. In Table 5, the absolute errors for the SSDT and TSDT are < 0.0078% and 0.0064%, respectively. From Tables 2–5, it can be observed that the errors under fully clamped boundary conditions are larger than those under completely free boundary conditions. The natural frequencies of the torsion modes are independent of the thickness (second and eighth modes in Tables 2 and 3 and the seventh and 16th modes in Tables 4 and 5). In Tables 2 and 3, the absolute errors for the TSDT and SSDT are similar for the clamped boundary. However, from Tables 4 and 5, the absolute errors for the TSDT are smaller than that for SSDT. We believe that as the radius-to-thickness ratio become smaller, more accurate result can be obtained base on the TSDT theory.

Figs. 2 and 3 show the selected mode shapes of the piezoceramic disk with fully clamped boundary conditions for $R/H = 10$ and $R/H = 5$, respectively. Figs. 4 and 5 show the selected mode shapes of the piezoceramic disk with completely free boundary conditions for $R/H = 10$ and $R/H = 5$, respectively. The mode shapes in the three directions are shown as obtained from COMSOL, SSDT and TSDT. The bold and black lines represent the nodal lines in the mode shapes obtained from COMSOL. The red and green regions represent the positive and negative displacements, respectively, in the mode shapes obtained from the theories. The bold and black

Table 4 The first ten natural frequencies (Hz) obtained from COMSOL and plate theories for a plate with free boundary conditions ($R/H = 10$).

Mode	(n, c)	COMSOL	SSDT	Error (%)	TSDT	Error (%)
1	(2,0)	23 136	23 135	−0.0043	23 136	0.0000
2	(1,0)	27 034	27 032	−0.0074	27 034	0.0000
3	(0,0)	34 497	34 497	0.0000	34 497	0.0000
4	(3,1)	35 527	35 521	−0.0169	35 527	0.0000
5	(2,0)	41 979	41 934	−0.1072	41 979	0.0000
6	(4,0)	46 269	46 265	−0.0086	46 269	0.0000
7	(0,0)	50 651	50 651	0.0000	50 651	0.0000
8	(5,0)	56 341	56 317	−0.0426	56 341	0.0000
9	(3,1)	57 682	57 680	−0.0035	57 682	0.0000
10	(1,1)	59 183	59 168	−0.0253	59 183	0.0000
11	(6,0)	66 082	66 078	−0.0061	66 082	0.0000
12	(1,0)	67 555	67 556	0.0015	67 555	0.0000
13	(4,1)	73 510	73 055	−0.6190	73 510	0.0000
14	(2,1)	75 574	75 567	−0.0093	75 574	0.0000
15	(7,0)	75 638	75 597	−0.0542	75 638	0.0000
16	(0,2)	83 017	83 017	0.0000	83 017	0.0000
17	(8,0)	85 078	85 092	0.0165	85 078	0.0000
18	(2,2)	87 030	87 040	0.0115	87 030	0.0000
19	(5,1)	89 058	89 035	−0.0258	89 058	0.0000
20	(3,1)	89 334	89 308	−0.0291	89 334	0.0000
21	(0,1)	90 382	90 379	−0.0033	90 382	0.0000
22	(9,0)	94 439	94 389	−0.0529	94 439	0.0000
23	(1,2)	98 140	98 138	−0.0020	98 139	-0.0010

Table 5 The first ten natural frequencies (Hz) obtained from COMSOL and plate theories for a plate with free boundary conditions ($R/H = 5$).

Mode	(n, c)	COMSOL	SSDT	Error (%)	TSDT	Error (%)
1	(2,0)	23 136	23 136	0.0000	23 137	0.0043
2	(1,0)	27 030	27 030	0.0000	27 030	0.0000
3	(0,0)	34 464	34 464	0.0000	34 464	0.0000
4	(3,0)	35 526	35 526	0.0000	35 526	0.0000
5	(2,0)	41 962	41 962	0.0000	41 962	0.0000
6	(4,0)	46 265	46 265	0.0000	46 265	0.0000
7	(0,1)	50 651	50 651	0.0000	50 651	0.0000
8	(5,1)	56 331	56 331	0.0000	56 331	0.0000
9	(3,1)	57 641	57 642	0.0017	57 642	0.0017
10	(1,2)	59 075	59 076	0.0017	59 075	0.0000
11	(6,0)	66 065	66 065	0.0000	66 065	0.0000
12	(1,0)	67 520	67 520	0.0000	67 520	0.0000
13	(4,1)	73 433	73 434	0.0014	73 434	0.0014
14	(2,1)	75 457	75 459	0.0027	75 458	0.0013
15	(7,0)	75 610	75 611	0.0013	75 610	0.0000
16	(0,2)	83 017	83 017	0.0000	83 017	0.0000
17	(8,0)	85 035	85 038	0.0035	85 037	0.0024
18	(2,2)	86 788	86 791	0.0035	86 789	0.0012
19	(5,1)	88 937	88 940	0.0034	88 938	0.0011
20	(3,1)	89 194	89 196	0.0022	89 195	0.0011
21	(0,1)	89 894	89 901	0.0078	89 896	0.0022
22	(9,0)	94 378	94 384	0.0064	94 384	0.0064
23	(1,2)	98 126	98 126	0.0000	98 126	0.0000

lines represent nodal lines. The ratios are the maximum displacements in the r and θ directions to the maximum displacement in the z direction. The theoretical ratios and mode shapes were in excellent agreement with the numerical calculations. It can be easily proven that the vibrations are in-plane dominated. However, for different thicknesses, even when the natural frequencies were similar, the ratios were different. For example, the natural frequencies of the first modes in Figs. 2 and 3 were similar. However, the ratio (TSDT) in the r direction in Fig. 2 is 40.958 while that in Fig. 3 is 20.497.

Figs. 6 and 7 show the selected figures of electric displacement D_z of the piezoceramic disk with fully clamped boundary conditions for $R/H = 10$ and $R/H = 5$, respectively. Figs. 8 and 9 show the selected of electric displacement D_z of the piezoceramic disk with completely free boundary conditions for $R/H = 10$ and $R/H = 5$, respectively.

The solution of electric displacement D_z based on SSDT can be expressed as

$$D_z = \left(\sum_{i=1}^{3} C_i \left(e_{31}\chi_i \hat{\Delta} + e_{33} - e_{31}\frac{\eta^2}{6}\hat{\Delta} \right) \hat{w}_{in}(\alpha_i \xi) \right) \cos(n\theta) e^{i\omega t} \tag{58}$$

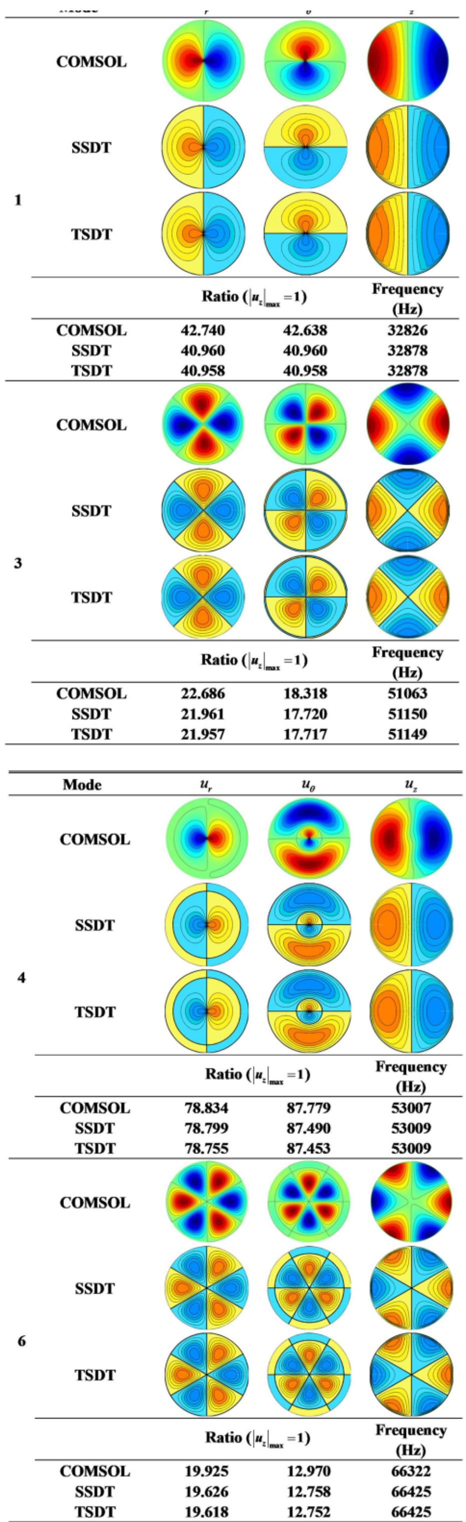

Figure 2 Selected mode shapes with clamped boundary condition $(R/H = 10)$.

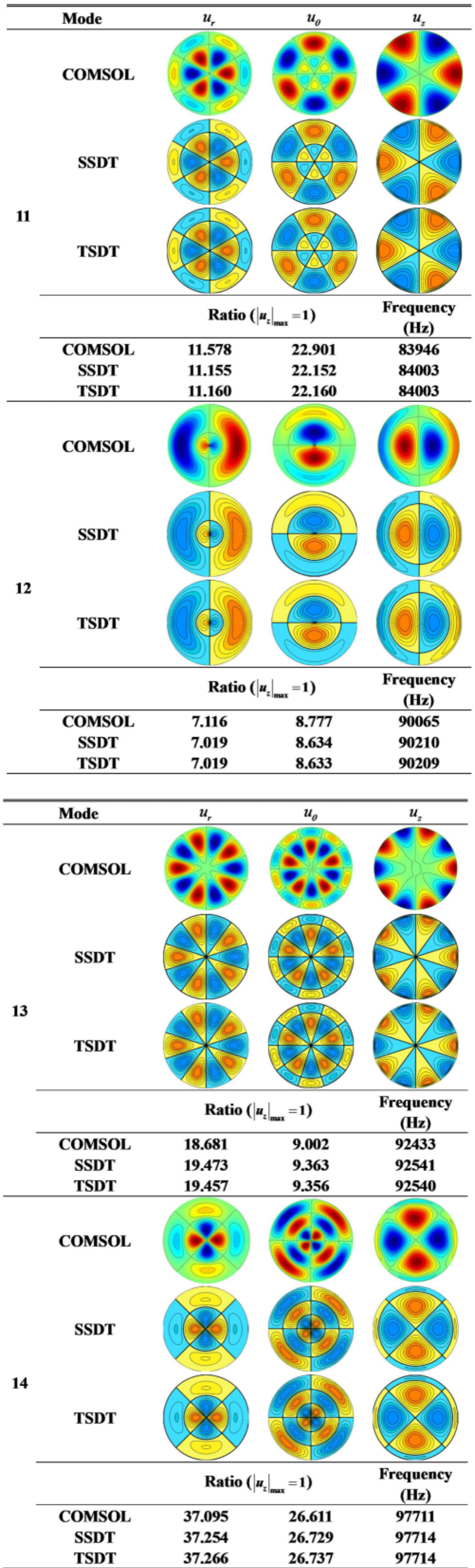

Figure 2 *Continued.*

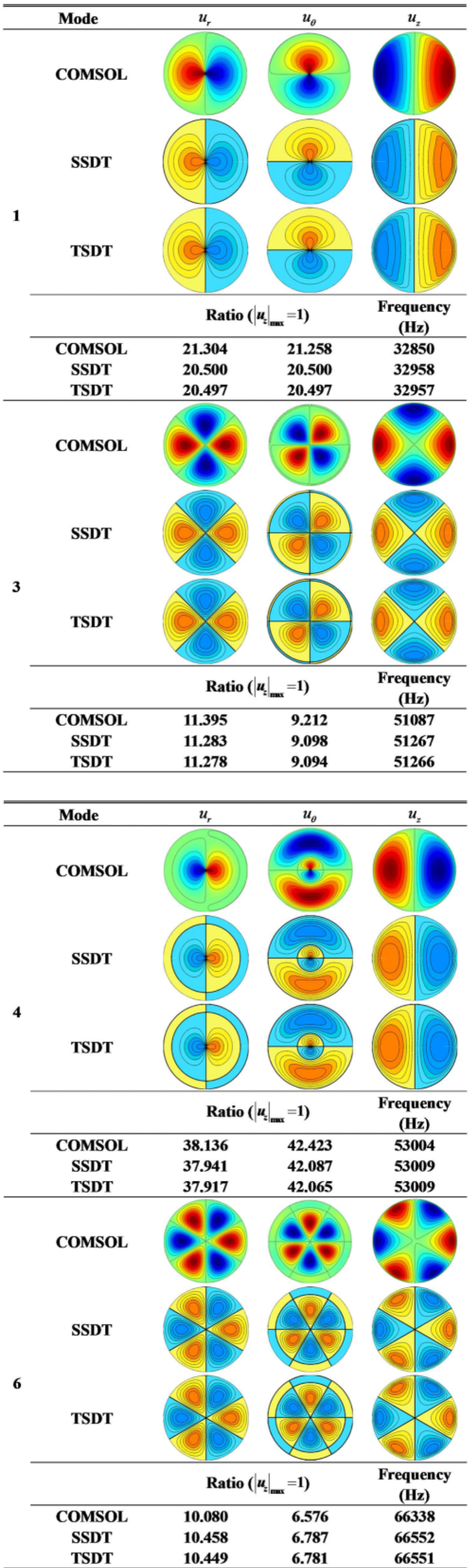

Figure 3 Selected mode shapes with clamped boundary condition ($R/H = 5$).

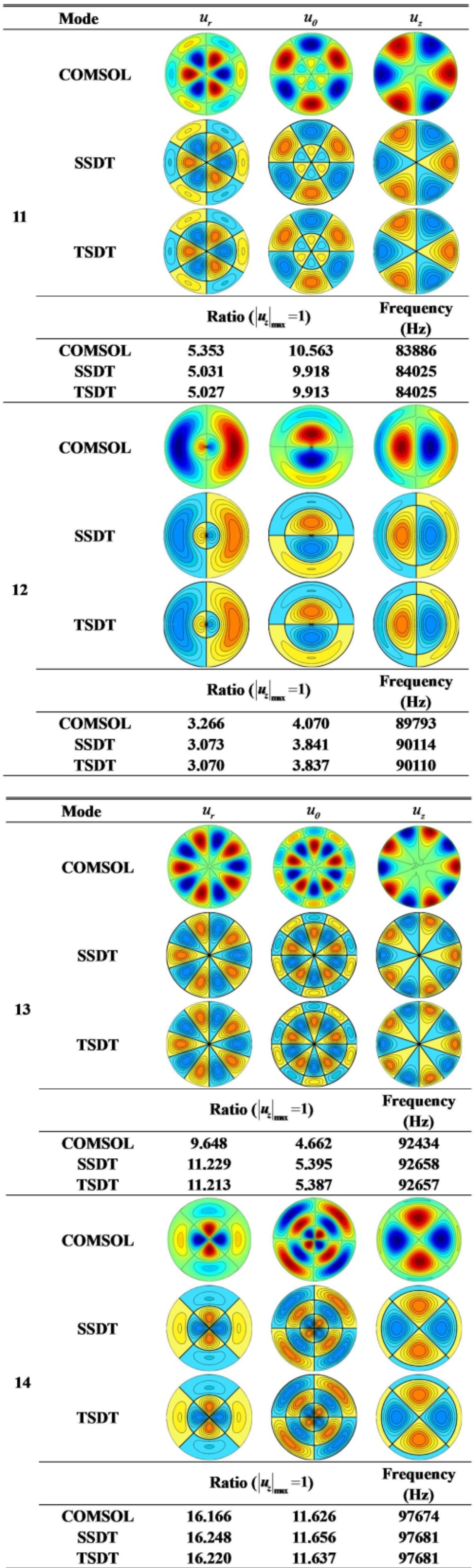

Figure 3 *Continued.*

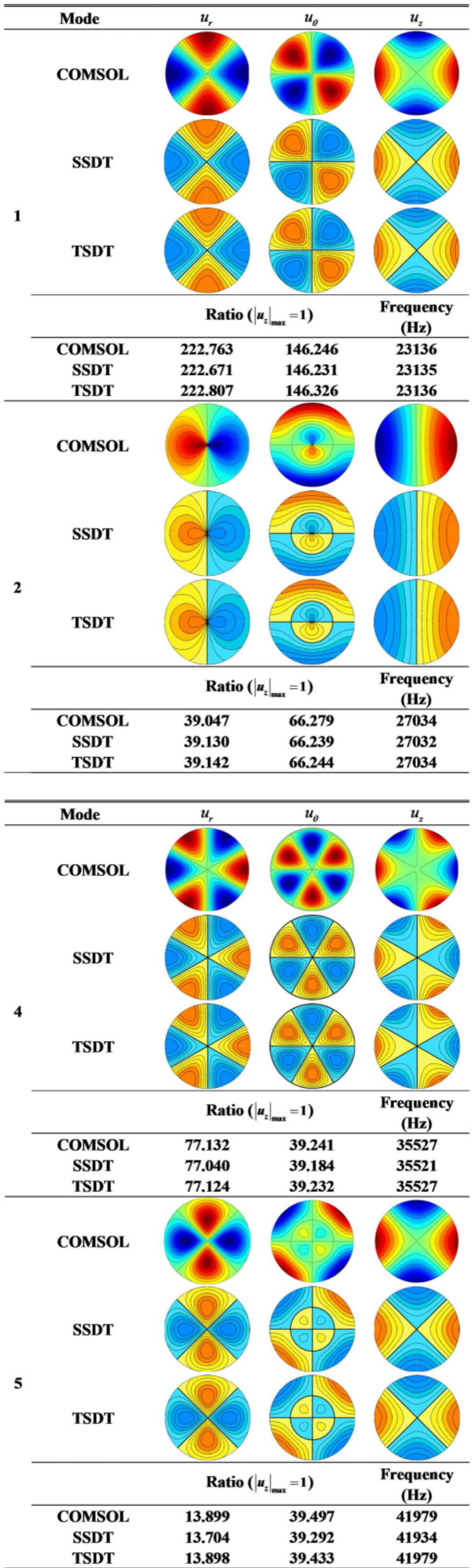

Figure 4 Selected mode shapes with free boundary condition ($R/H = 10$).

Mode		u_r	u_θ	u_z
19	COMSOL / SSDT / TSDT			

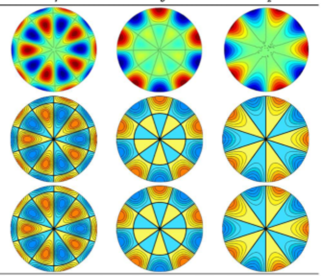

		Ratio ($\lvert u_z\rvert_{max}=1$)		Frequency (Hz)
19	COMSOL	6.435	17.004	89058
	SSDT	5.032	15.685	89035
	TSDT	6.432	16.861	89058

Mode		u_r	u_θ	u_z
20	COMSOL / SSDT / TSDT			

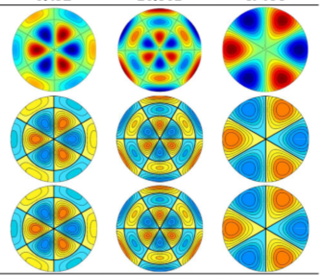

		Ratio ($\lvert u_z\rvert_{max}=1$)		Frequency (Hz)
20	COMSOL	21.977	15.481	89334
	SSDT	21.888	15.385	89308
	TSDT	21.933	15.426	89334

Mode		u_r	u_θ	u_z
22	COMSOL / SSDT / TSDT			

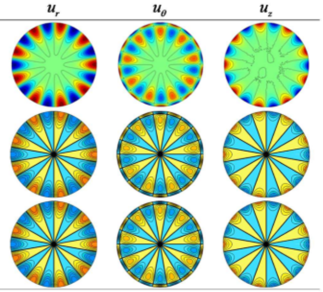

		Ratio ($\lvert u_z\rvert_{max}=1$)		Frequency (Hz)
22	COMSOL	15.243	7.314	94439
	SSDT	15.253	7.113	94389
	TSDT	15.266	7.117	94439

Mode		u_r	u_θ	u_z
23	COMSOL / SSDT / TSDT			

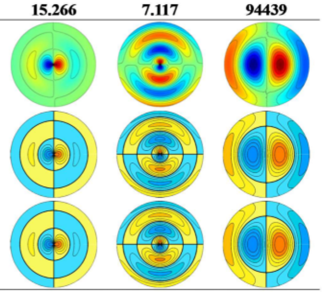

		Ratio ($\lvert u_z\rvert_{max}=1$)		Frequency (Hz)
23	COMSOL	81.438	81.928	98140
	SSDT	82.302	82.302	98138
	TSDT	82.382	82.382	98139

Figure 4 *Continued*.

Mode		u_r	u_θ	u_z
1	COMSOL / SSDT / TSDT			

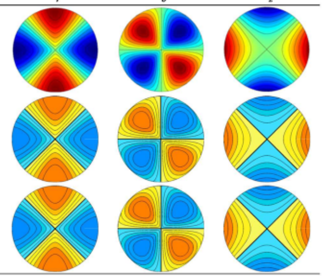

		Ratio ($\lvert u_z \rvert_{max} = 1$)		Frequency (Hz)
1	COMSOL	110.556	72.587	23136
1	SSDT	110.589	72.630	23136
1	TSDT	110.553	72.607	23137

Mode		u_r	u_θ	u_z
2	COMSOL / SSDT / TSDT			

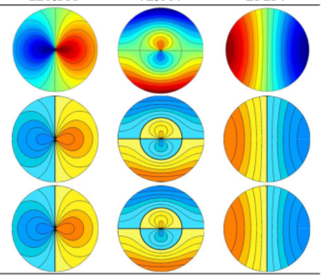

		Ratio ($\lvert u_z \rvert_{max} = 1$)		Frequency (Hz)
2	COMSOL	19.311	32.749	27030
2	SSDT	19.355	32.685	27030
2	TSDT	19.344	32.668	27030

Mode		u_r	u_θ	u_z
3	COMSOL / SSDT / TSDT			

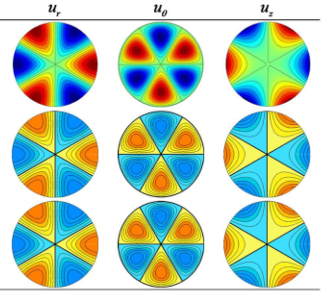

		Ratio ($\lvert u_z \rvert_{max} = 1$)		Frequency (Hz)
3	COMSOL	37.954	19.310	35526
3	SSDT	37.965	19.314	35526
3	TSDT	37.937	19.300	35526

Mode		u_r	u_θ	u_z
4	COMSOL / SSDT / TSDT			

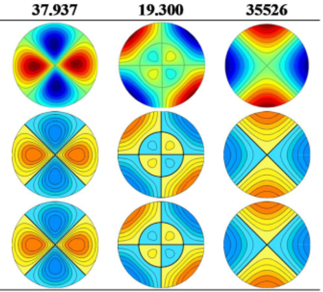

		Ratio ($\lvert u_z \rvert_{max} = 1$)		Frequency (Hz)
4	COMSOL	6.775	19.216	41962
4	SSDT	6.772	19.103	41962
4	TSDT	6.763	19.078	41962

Figure 5 Selected mode shapes with free boundary condition ($R/H = 5$).

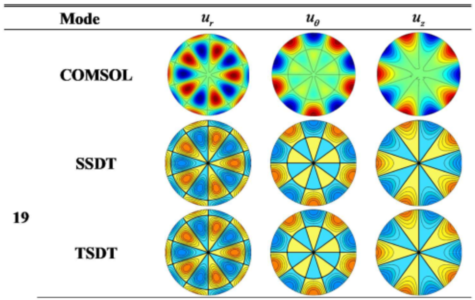

	Ratio ($\lvert u_z \rvert_{max}=1$)		Frequency (Hz)
COMSOL	2.808	7.518	88937
SSDT	2.819	7.294	88940
TSDT	2.793	7.240	88938

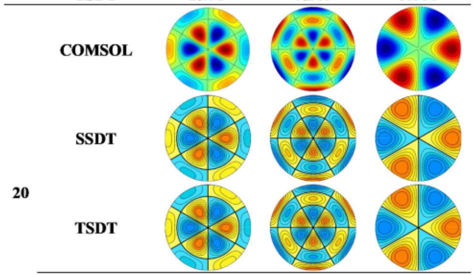

	Ratio ($\lvert u_z \rvert_{max}=1$)		Frequency (Hz)
COMSOL	9.868	6.903	89194
SSDT	9.783	6.793	89196
TSDT	9.773	6.785	89195

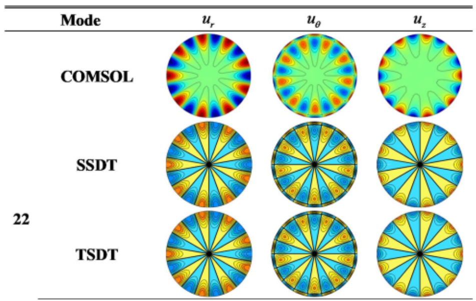

	Ratio ($\lvert u_z \rvert_{max}=1$)		Frequency (Hz)
COMSOL	7.103	3.412	94378
SSDT	7.244	3.098	94384
TSDT	7.216	3.084	94384

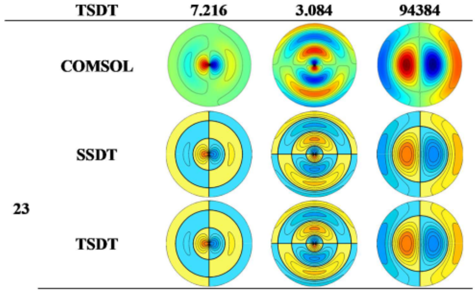

	Ratio ($\lvert u_z \rvert_{max}=1$)		Frequency (Hz)
COMSOL	35.134	35.344	98126
SSDT	35.473	35.473	98126
TSDT	35.414	35.414	98126

Figure 5 *Continued*.

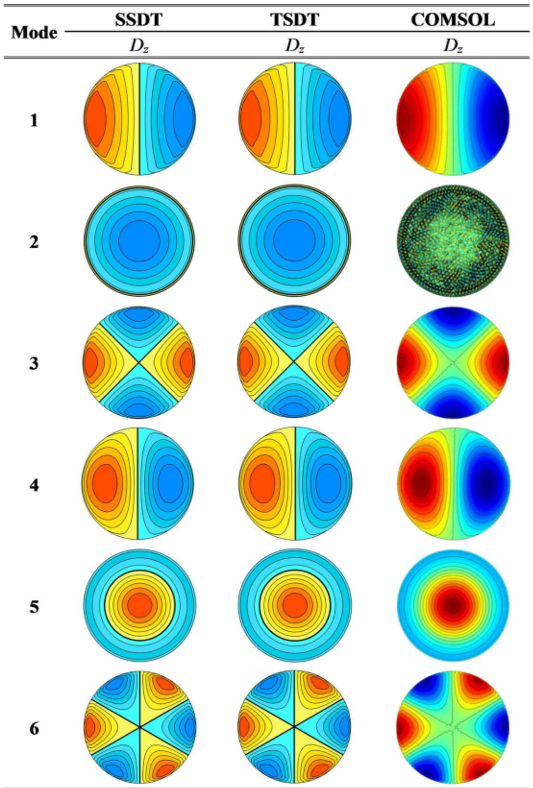

Figure 6 First six electric displacements along z-direction for clamped boundary condition ($R/H = 10$).

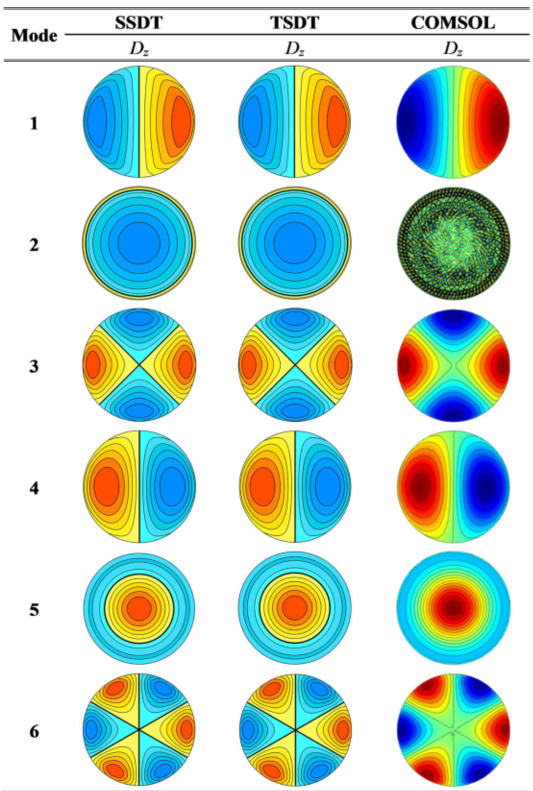

Figure 7 First six electric displacements along z-direction for clamped boundary condition ($R/H = 5$).

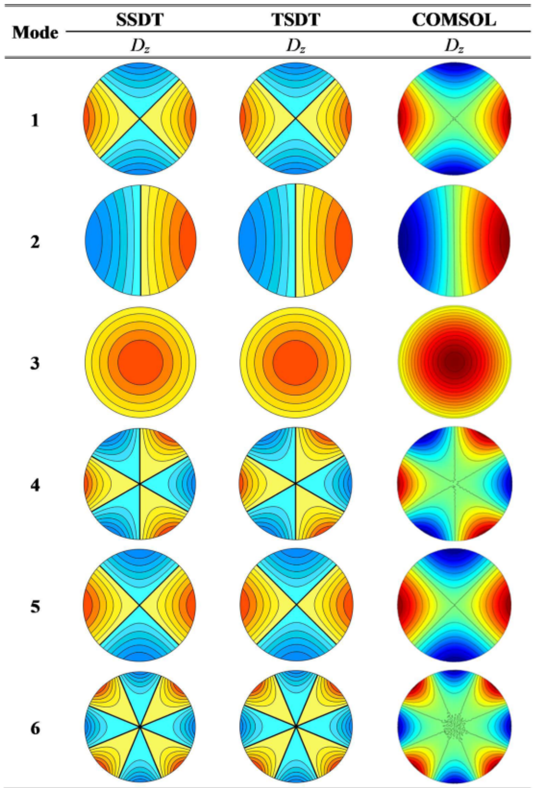

Figure 8 First six electric displacements along z-direction for free boundary condition $(R/H = 10)$.

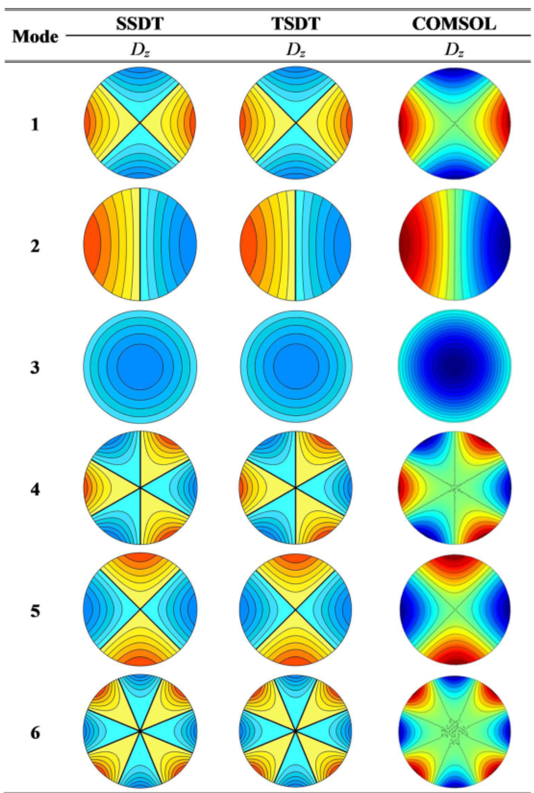

Figure 9 First six electric displacements along z-direction for free boundary condition $(R/H = 5)$.

The solution of electric displacement D_z based on TSDT can be expressed as

$$D_z = \left(\sum_{i=1}^{3} C_i \left(e_{31} \chi_i \hat{\Delta} + e_{33} (1 + \lambda_i \eta^2) - e_{31} \frac{\eta^2}{6} (1 + \lambda_i \eta^2) \hat{\Delta} \right) \hat{w}_{in} (\alpha_i \xi) \right) \cos(n\theta) e^{i\omega t} \tag{59}$$

The theoretical mode shapes of electric displacement D_z were in excellent agreement with the numerical calculations for different thickness and boundary conditions. It can be observed that the distribution of electric displacements D_z are similar with those mode shapes in the z direction. This result implies that the designs of surface electrodes for exciting specific in-plane mode shapes can be referred to the associated distributions of displacement function u_z. Furthermore, the comparison results in Figs. 6 and 7 indicate that the analytical method can give more stable and convergence physical quantities of displacement and electric properties than numerical calculation results.

5. CONCLUSIONS

In this study, the authors present two higher-order plate theories: SSDT and TSDT, and simplified third-order linear piezoelectric theory to study the in-plane dominated vibrations of thick piezoelectric circular plates under fully clamped and completely free boundary conditions. Hamilton's principle and the variation method were applied to derive the equations of motion and boundary conditions. In theoretical analysis, the resonant frequencies, associated mode shapes and shapes of electric distribution for various radius-to-thickness ratios were calculated. The numerical results obtained by the FEM were compared with those obtained from theoretical analysis. The two higher-order shear deformation plate theories and simplified third-order linear piezoelectric theory can accurately predict the resonant frequencies and mode shapes. The proposed theories have been verified by comparison with FEM. The proposed theories will be applied to study the in-plane dominated vibrations of thick piezoelectric rectangular plates analytically, especially under completely free boundary conditions. The work is now in progress.

ACKNOWLEDGEMENTS

The author, C-C.M., would like to express his gratitude to Professor Chau-Shioung Yeh for the long relationship as a friend and constant guidance as a mentor in the past 35 years. Professor Yeh and I are all working in the general field of wave mechanics and I learned a lot from him and would like to express my deepest appreciation with great respect. Professor Yeh had made extraordinary contributions to the development and application of earthquake engineering in Taiwan. He also made significant contribution for the Society of Theoretical and Applied Mechanics. The authors would like to dedicate this paper to the memory of Professor Chau-Shioung Yeh for his important contribution to the mechanics society in Taiwan and we all miss him.

The authors gratefully acknowledge the financial support for this study by the Ministry of Science and Technology (Republic of China) under Grants MOST 107–2221-E-002–086-MY3 and MOST 109–2222-E-194–001-MY2.

APPENDIX A

Case 1 clamped boundary condition ($i = 1 - 3$):

$$S_{1i}^S = \hat{w}_{in}(\alpha_i) \tag{A.1}$$

$$S_{14}^S = 0 \tag{A.2}$$

$$S_{2i}^S = \frac{\partial \hat{w}_{in}(\alpha_i)}{\partial \xi} \tag{A.3}$$

$$S_{24}^S = 0 \tag{A.4}$$

$$S_{2i}^S = \chi_i \frac{\partial \hat{w}_{in}(\alpha_i)}{\partial \xi} \tag{A.5}$$

$$S_{34}^S = n\hat{w}_{4n}(\alpha_4) \tag{A.6}$$

$$S_{4i}^S = \chi_i n\hat{w}_{in}(\alpha_i) \tag{A.7}$$

$$S_{44}^S = \frac{\partial \hat{w}_{4n}(\alpha_4)}{\partial \xi} \tag{A.8}$$

Case 2 free boundary condition $(i = 1 - 3)$:

$$S_{1i}^{S} = \left(\chi_i - \frac{3}{10}\eta^2\right)\left(\frac{\partial^3 \hat{w}_{in}(\alpha_i)}{\partial \xi^3} + \frac{\partial^2 \hat{w}_{in}(\alpha_i)}{\partial \xi^2}\right) + \Big(-\chi_i\left(n^2+1\right) - (1-\gamma_{12})\chi_i n^2 + \frac{3}{10}\eta^2(1-\gamma_{12})n^2 + \frac{3}{10}\eta^2\left(1+n^2\right) + \gamma_{13} - \frac{4}{5}\eta^2 x_i n_{31} + \lambda^4\chi_i - \frac{3}{10}\eta^2\lambda^4\Big)\frac{\partial \hat{w}_{in}(\alpha_i)}{\partial \xi} + (3-\gamma_{12})\left(\chi_i - \frac{3}{10}\eta^2\right)n^2\hat{w}_{in}(\alpha_i) \tag{A.9}$$

$$S_{14}^{S} = \left(-n^3(1-\gamma_{12}) + \lambda^4 n\right)\hat{w}_{4n}(\alpha_4) + (1-\gamma_{12})\,n\frac{\partial \hat{w}_{4n}(\alpha_4)}{\partial \xi} \tag{A.10}$$

$$S_{2i}^{S} = \left(\chi_i - \frac{3}{10}\eta^2\right)\left(\frac{\partial^2 \hat{w}_{in}(\alpha_i)}{\partial \xi^2} + \gamma_{12}\frac{\partial \hat{w}_{in}(\alpha_i)}{\partial \xi} - \gamma_{12}n^2\hat{w}_{in}(\alpha_i)\right) + \left(\gamma_{13} - \frac{4}{5}\eta^2 x_i n_{31}\right)\hat{w}_{in}(\alpha_i) \tag{A.11}$$

$$S_{24}^{S} = (1-\gamma_{12})\,n\left(\frac{\partial \hat{w}_{4n}(\alpha_4)}{\partial \xi} - \hat{w}_{4n}(\alpha_4)\right) \tag{A.12}$$

$$S_{3i}^{S} = \left(\chi_i - \frac{\eta^2}{6}\right)\left(\frac{\partial^2 \hat{w}_{in}(\alpha_i)}{\partial \xi^2} + \gamma_{12}\frac{\partial \hat{w}_{in}(\alpha_i)}{\partial \xi} - \gamma_{12}n^2\hat{w}_{in}(\alpha_i)\right) + \gamma_{13}\hat{w}_{in}(\alpha_i) \tag{A.13}$$

$$S_{34}^{S} = (1-\gamma_{12})\,n\left(\frac{\partial \hat{w}_{4n}(\alpha_4)}{\partial \xi} - \hat{w}_{4n}(\alpha_4)\right) \tag{A.14}$$

$$S_{4i}^{S} = n\left(2\chi_i - \frac{\eta^2}{3}\right)\left(-\frac{\partial \hat{w}_{in}(\alpha_i)}{\partial \xi} + \hat{w}_{in}(\alpha_i)\right) \tag{A.15}$$

$$S_{44}^{S} = -n^2\hat{w}_{4n}(\alpha_4) + \frac{\partial \hat{w}_{4n}(\alpha_4)}{\partial \xi} - \frac{\partial^2 \hat{w}_{4n}(\alpha_4)}{\partial^2 \xi} \tag{A.16}$$

APPENDIX B

Case 1 clamped boundary condition $(i = 1 - 4)$:

$$S_{1i}^{T} = \hat{w}_{in}(\alpha_i) \tag{B.1}$$

$$S_{15}^{T} = 0 \tag{B.2}$$

$$S_{2i}^{T} = \lambda_i\hat{w}_{in}(\alpha_i) \tag{B.3}$$

$$S_{25}^{T} = 0 \tag{B.4}$$

$$S_{3i}^{T} = (1+\eta^2\lambda_i)\frac{\partial \hat{w}_{in}(\alpha_i)}{\partial \xi} \tag{B.5}$$

$$S_{35}^{T} = 0 \tag{B.6}$$

$$S_{4i}^{T} = \chi_i\frac{\partial \hat{w}_{in}(\alpha_i)}{\partial \xi} \tag{B.7}$$

$$S_{45}^{T} = n\hat{w}_{5n}(\alpha_5) \tag{B.8}$$

$$S_{5i}^{T} = \chi_i n\hat{w}_{in}(\alpha_i) \tag{B.9}$$

$$S_{55}^{T} = \frac{\partial \hat{w}_{5n}(\alpha_5)}{\partial \xi} \tag{B.10}$$

Case 2 free boundary condition $(i = 1 - 4)$:

$$S_{1i}^{T} = \chi_i \frac{\partial \hat{w}_{in}(\alpha_i)}{\partial \xi} \tag{B.11}$$

$$S_{15}^{T} = 0 \tag{B.12}$$

$$\begin{aligned} S_{2i}^{T} = &\left(\chi_i - \frac{3}{10}\eta^2 - \frac{3}{10}\eta^4\lambda_i\right)\left(\frac{\partial^3 \hat{w}_{in}(\alpha_i)}{\partial \xi^3} + \frac{\partial^2 \hat{w}_{in}(\alpha_i)}{\partial \xi^2}\right. \\ &\left. + \left(\lambda^4 - \left(n^2+1\right) - \left(1-\gamma_{12}\right)n^2\right)\frac{\partial \hat{w}_{in}(\alpha_i)}{\partial \xi} + \left(3-\gamma_{12}\right)n^2 \hat{w}_{in}(\alpha_i)\right) \end{aligned} \tag{B.13}$$

$$\left(\gamma_{13} + \left(\frac{9}{5}\gamma_{13} + \frac{4}{5}m_1\right)\eta^2\lambda_i - \frac{2}{15}m_2 x_i \eta^2\left(1+\eta^2\lambda_i\right)\right)\frac{\partial \hat{w}_{in}(\alpha_i)}{\partial \xi}$$

$$S_{25}^{T} = \left(-n^3(1-\gamma_{12}) + \lambda^4 n\right)\hat{w}_{5n}(\alpha_5) + (1-\gamma_{12})n\frac{\partial \hat{w}_{5n}(\alpha_5)}{\partial \xi} \tag{B.14}$$

$$\begin{aligned} S_{3i}^{T} = &\left(\chi_i - \frac{3}{10}\eta^2 - \frac{3}{10}\eta^4\lambda_i\right)\left(\frac{\partial^2 \hat{w}_{in}(\alpha_i)}{\partial \xi^2} + \gamma_{12}\frac{\partial \hat{w}_{in}(\alpha_i)}{\partial \xi} - \gamma_{12}n^2\hat{w}_{in}(\alpha_i)\right) \\ &+ \left(\gamma_{13} + \left(\frac{9}{5}\gamma_{13} + \frac{4}{5}m_1\right)\eta^2\lambda_i - \frac{2}{15}m_2 x_i\eta^2\left(1+\eta^2\lambda_i\right)\right)\hat{w}_{in}(\alpha_i) \end{aligned} \tag{B.15}$$

$$S_{35}^{T} = \left(1-\gamma_{12}\right)n\left(\frac{\partial \hat{w}_{5n}(\alpha_5)}{\partial \xi} - \hat{w}_{5n}(\alpha_5)\right) \tag{B.16}$$

$$\begin{aligned} S_{4i}^{T} = &\left(\chi_i - \frac{\eta^2}{6} - \frac{\eta^4}{6}\lambda_i\right)\left(\frac{\partial^2 \hat{w}_{in}(\alpha_i)}{\partial \xi^2} + \gamma_{12}\frac{\partial \hat{w}_{in}(\alpha_i)}{\partial \xi} - \gamma_{12}n^2\hat{w}_{in}(\alpha_i)\right) \\ &+ \gamma_{13}\left(1+\eta^2\lambda_i\right)\hat{w}_{in}(\alpha_i) \end{aligned} \tag{B.17}$$

$$S_{45}^{T} = \left(1-\gamma_{12}\right)n\left(\frac{\partial \hat{w}_{5n}(\alpha_5)}{\partial \xi} - \hat{w}_{5n}(\alpha_5)\right) \tag{B.18}$$

$$S_{5i}^{T} = n\left(2\chi_i - \frac{\eta^2}{3} - \frac{\eta^4}{3}\lambda_i\right)\left(-\frac{\partial \hat{w}_{in}(\alpha_i)}{\partial \xi} + \hat{w}_{in}(\alpha_i)\right) \tag{B.19}$$

$$S_{55}^{T} = -n^2\hat{w}_{5n}(\alpha_5) + \frac{\partial \hat{w}_{5n}(\alpha_5)}{\partial \xi} - \frac{\partial^2 \hat{w}_{5n}(\alpha_5)}{\partial^2 \xi} \tag{B.20}$$

REFERENCES

1. Mindlin RD. Forced thickness-shear and flexural vibrations of piezoelectric crystal plates. *The Journal of Applied Physics* 1952;**23**(1):83–88.
2. Tiersten HF, Mindlin RD. Forced vibrations of piezoelectric crystal plates. *Quaterly of Applied Mathematics* 1962;**20**(2):107–119.
3. Holland R. Contour extensional resonant properties of rectangular piezoelectric plates. *IEEE Transactions of Sonics and Ultrasonics* 1968;**15**(2):97–104.
4. Schmidt GH. Extensional vibrations of piezoelectric plates. *Journal of Engineering Mathematics* 1972;**6**(2):133–142.
5. Schmidt GH. Application of the finite element method to the extensional vibrations of piezoelectric plates. *The Mathematics of Finite Elements and Applications*. Academic Press, 1973, 351–366.
6. Ikegami S, Ueda I, Kobayashi S. Frequency spectra of resonant vibration in disk plates of $PbTiO_3$ piezoelectric ceramics. *The Journal of Acoustical Society of America* 1974;**55**(2):339–344.
7. Ueha S, Sakuma S, Mori E. Measurement of vibration velocity distributions and mode analysis in thick disks of $Pb(Zr \cdot Ti)O_3$. *The Journal of Acoustical Society of America* 1983;**73**(5):1842–1847.
8. Locke S, Kunkel HA, Pikeroen B. Finite element modelling of piezoelectric ceramic disks. *IEEE 1987 Ultrasonics Symposium*. IEEE 1987:701–706.
9. Ohnishi, Kishie, Iwamoto, Sasaki, Zaitsu, Inoue Piezoelectric ceramic transformer operating in thickness extensional vibration mode for power supply. *IEEE 1992 Ultrasonics Symposium Proceedings*. IEEE 1992:483–488.
10. Guo N, Cawley P, Hitchings D. The finite element analysis of the vibration characteristics of piezoelectric discs. *Journal of Sound and Vibrations* 1992;**159**(1):115–138.
11. Lee PCY, Edwards NP. Extensional vibrations of piezoelectric crystal plates and strips. *Proceedings of the 1999 Joint Meeting of the European Frequency and Time Forum and the IEEE International Frequency Control Symposium (Cat. No. 99CH36313)*. IEEE 1999:754–757.
12. Huang, Lee, Lin, Yu Extensional, thickness-stretch and symmetric thickness-shear vibrations of piezoceramic disks. *IEEE Transactions Ultrasonics, Ferroelectric Frequency Control* 2002;**49**(11):1507–1515.
13. Ma CC, Huang CH. The investigation of three-dimensional vibration for piezoelectric rectangular parallelepipeds using the AF-ESPI method. *IEEE Transactions Ultrasonics, Ferroelectric Frequency Control* 2001;**48**:142–153.

14. Ma CC, Huang CH. Experimental full field investigations of resonant vibrations for piezoceramic plates by an optical interferometry method. *Experimental Mechanics* 2002;**42**(2):140–146.
15. Huang CH, Ma CC. Experimental and numerical investigations of resonant vibration characteristics for piezoceramic plates. *The Journal of Acoustical Society of America* 2001;**109**(6):2780–2788.
16. Lin YC, Ma CC. Experimental measurement and numerical analysis on resonant characteristics of piezoelectric disks with partial electrode designs. *IEEE Transactions Ultrasonics, Ferroelectric Frequency Control* 2004;**51**:937–947.
17. Huang CH, Ma CC, Lin YC. Theoretical, numerical, and experimental investigation on resonant vibrations of piezoceramic annular disks. *IEEE Transactions Ultrasonics, Ferroelectric Frequency Control* 2005;**52**(8):1204–1216.
18. Ma CC, Lin YC, Lin HY. Dynamic in-plane resonant characteristics of piezoceramic and piezolaminated composite plates. *IEEE Transactions Ultrasonics, Ferroelectric Frequency Control* 2008;**55**:526–537.
19. Huang, Li, Wu, Ma Theoretical analysis of transverse and planar vibrations for the piezoceramic disk based on Mindlin plate theory. *Applied Mathematical Modelling* 2021;**97**:568–587.
20. Chillara VK, Hakoda C, Pantea C. On the in-plane vibrations and electromechanical resonance characteristics of non-uniformly polarized rectangular piezoelectric wafers: Selective mode-type excitation and specific mode enhancement. *Journal of Sound and Vibrations* 2021;**506**:116129.
21. Lin, Huang, Ma, Chang Experimental and theoretical investigations on sensing and dynamic characteristics of PVDF thin film. *Journal of Mechanics*, 2021;**37**:1–12.
22. Yang JH, Fu G, Sun GF. Bifurcation and chaos of BNNT-reinforced piezoelectric plate under complex load. *Journal of Mechanics*, 2021;**37**:230–241.
23. Ji M, Wu YC, Ma CC. Analytical solutions for in-plane dominated vibrations of transversely isotropic circular plates based on high-order theories. *Journal of Sound and Vibrations*, 2021;**503**:116110.